PAPER • OPEN ACCESS

Overview of the SPARC physics basis towards the exploration of burning-plasma regimes in high-field, compact tokamaks

View the article online for updates and enhancements.

Overview of the SPARC physics basis towards the exploration of burning-plasma regimes in high-field, compact tokamaks

P. Rodriguez-Fernandez[1],[*] , A.J. Creely[2] , M.J. Greenwald[1] ,
D. Brunner[2], S.B. Ballinger[1] , C.P. Chrobak[2] , D.T. Garnier[1] ,
R. Granetz[1] , Z.S. Hartwig[1], N.T. Howard[1] , J.W. Hughes[1] , J.H. Irby[1],
V.A. Izzo[3] , A.Q. Kuang[1], Y. Lin[1], E.S. Marmar[1], R.T. Mumgaard[2],
C. Rea[1] , M.L. Reinke[2] , V. Riccardo[2] , J.E. Rice[1] , S.D. Scott[2] ,
B.N. Sorbom[2] , J.A. Stillerman[1], R. Sweeney[1] , R.A. Tinguely[1] ,
D.G. Whyte[1], J.C. Wright[1] and D.V. Yuryev[2]

[1] MIT Plasma Science and Fusion Center, Cambridge, United States of America
[2] Commonwealth Fusion Systems, Cambridge, United States of America
[3] Fiat Lux, San Diego, United States of America

E-mail: pablorf@mit.edu

CrossMark

Abstract

The SPARC tokamak project, currently in engineering design, aims to achieve *breakeven* and burning plasma conditions in a compact device, thanks to new developments in high-temperature superconductor technology. With a magnetic field of 12.2 T on axis and 8.7 MA of plasma current, SPARC is predicted to produce 140 MW of fusion power with a plasma gain of $Q \approx 11$, providing ample margin with respect to its mission of $Q > 2$. All tokamak systems are being designed to produce this landmark plasma discharge, thus enabling the study of burning plasma physics and tokamak operations in reactor relevant conditions to pave the way for the design and construction of a compact, high-field fusion power plant. Construction of SPARC is planned to begin by mid-2021.

(Some figures may appear in colour only in the online journal)

1. Introduction

The development of high-temperature superconductors (HTS) in recent years is driving a revolution in fusion science and technology [1, 2]. The use of high magnetic fields to confine plasmas in both tokamak and stellarator designs leads to more stability and better performance. Reducing machine size by increasing the magnetic field intensity results in burning plasma experiments that are generally easier and faster to build and fusion power plant concepts that are economically attractive. Thanks to this, the construction of a US fusion pilot plant at low capital cost in the near-term becomes feasible and is in line with the recommendations from the National Academies of Sciences, Engineering and Medicine [3, 4], the American Physical Society [5] and the DOE Fusion Energy Sciences Advisory Committee [6] culminating from a long-range strategic planning process. The development of economically attractive fusion power plants based on HTS technology is critical for the timely, large-scale adoption of fusion energy to mitigate the effects of climate change.

[*] Author to whom any correspondence should be addressed.

The MIT Plasma Science and Fusion Centre and the private company Commonwealth Fusion Systems (CFS) are now finalizing the design of SPARC [7], a demonstration device aimed at fusing deuterium (D) and tritium (T) and exceeding *breakeven* plasma conditions, that is, to create and confine plasmas that produce more power by fusion reactions than absorbed from the external heating systems. This milestone, never achieved in a controlled magnetic confinement fusion device to date, will allow the study of net-energy plasmas regimes and the demonstration of HTS magnet technology integrated with the rest of tokamak systems at reactor-relevant conditions. This demonstration will pave the way towards the construction of a compact pilot plant, largely based on the ARC concept [8, 9], by the second half of the next decade.

This paper presents the status of the SPARC project (section 2) and a description of the main scenarios that SPARC is designed to achieve (section 3). The core plasma physics of the main net-energy scenario is discussed (section 4), as well as the heat flux handling (section 5) and disruption mitigation (section 6) strategies that are currently planned. Lastly, conclusions (section 7) are presented.

2. Project status

The first conceptual version of SPARC was originally presented to the community at the 60th Annual Meeting of the APS Division of Plasma Physics in 2018 [10] and consisted of a moderately-shaped machine of the size of ASDEX Upgrade with a toroidal magnetic field of 12 T on axis. A higher confidence in the HTS coil development, along with an increase in fusion gain margin and further refinements to the inner radial build resulted in an updated version of the SPARC design. The physics basis of this version of the SPARC tokamak was recently published, including an overview of the machine [7] and explorations of numerous physics topics: core transport and performance [11], H-mode access and edge pedestal physics [12], divertor heat flux challenge and mitigation [13], ICRF system [14], MHD stability and disruptions [15] and fast ion physics [16].

The SPARC tokamak is under design as a compact, pulsed, high-field, D–T fusing, tungsten-walled tokamak with the primary goal of demonstrating operation with a fusion gain of $Q = P_{fus}/P_{in} > 2$, where P_{fus} is the total fusion power and P_{in} is the power absorbed in the plasma. Apart from moderate ohmic heating, SPARC will utilize ion cyclotron range-of-frequencies (ICRF) heating to deliver a maximum of $P_{ICRF} = 25$ MW of coupled power to the plasma. Table 1 presents the main tokamak and plasma parameters, and figure 1(*a*) presents the poloidal cross section of the device. The use of a high magnetic field on-axis ($B_T = 12.2$ T) will allow stable operation with high plasma current ($I_p = 8.7$ MA) and high absolute density ($\langle n_e \rangle = 3.1 \times 10^{20}$ m^{-3}). The high values of these two parameters lead to high confinement and high fusion power in a compact machine ($R_0 = 1.85$ m, $a = 0.57$ m).

The SPARC project is well underway and will enter the construction phase in the second half of 2021, after successful demonstration of a toroidal field model coil (TFMC), which

Table 1. Main tokamak and nominal plasma parameters of SPARC. For details on definitions, consult reference [7].

Parameter	Value
B_T	12.2 T
I_p	8.7 MA
R_0	1.85 m
a	0.57 m
κ_{sep}, κ_a	1.97, 1.75
δ_{sep}	0.54
$P_{ICRF, max}$	25 MW
$\langle n_e \rangle$	3.1×10^{20} m^{-3}
$\Delta t_{flattop}$	10 s
ϕ_{tot}	42 Wb
q^*_{Uckan}	3.05
f_G	0.37

scientists and engineers at MIT and CFS have been developing over the last three years. Tests at SPARC-relevant electromagnetic loading of high-current cables manufactured with HTS have shown excellent performance [17–19]. The goal of the TFMC is to demonstrate the magnet technology required for SPARC toroidal field coils. Construction and commissioning of SPARC is projected to last four years, yielding a total of seven years from start of design to commissioning. This timeline is aggressive but consistent with previous experience with the two other D–T tokamaks built and operated, TFTR [20] and JET [21]. The SPARC tokamak will be sited in Devens, Massachusetts (USA), where CFS has started the construction of a 47-acre campus that will include advanced manufacturing and research facilities, as well as corporate offices and headquarters [22].

3. Main scenarios

For the initial scoping of tokamak scenarios and machine parameters, a conservative, empirically based, power-balance approach has been taken. This method is inspired by standard plasma operation contour (POPCON) analysis [23] and has been improved to account for a refined treatment of radiation from impurity ions and corrections to scaling laws for peaking and power threshold, among other aspects [7]. Figure 1(*b*) shows the nominal POPCON plot for SPARC with the machine parameters indicated in table 1. Within plasma physics and machine limits, a large operational space is found that exceeds the mission requirement $Q > 2$, with a maximum of $Q \approx 11$ when operated with a 50–50 mixture of D–T. For baseline performance predictions, a dilution of main ions of $n_{DT}/n_e = 0.85$ is assumed, as well as an effective ion charge of $Z_{eff} = 1.5$, as described in [7, 11]. A nominal concentration of tungsten of $n_W/n_e = 1.5 \times 10^{-5}$ is employed, consistent with what has been achieved in other tungsten-walled machines. This scenario, which will be referred to as the primary reference discharge (PRD), operates with a volume-averaged density of $\langle n_e \rangle = 3.1 \times 10^{20}$ m^{-3}, substantially below the Greenwald limit ($n_G = 8.4 \times 10^{20}$ m^{-3}) and low beta, $\beta_N = 1.05$. An energy confinement time of $\tau_E = 0.77$ s is estimated from the ITPA $\tau_{98,y2}$ scaling law [24] with an H-factor of $H_{98,y2} = 1.0$.
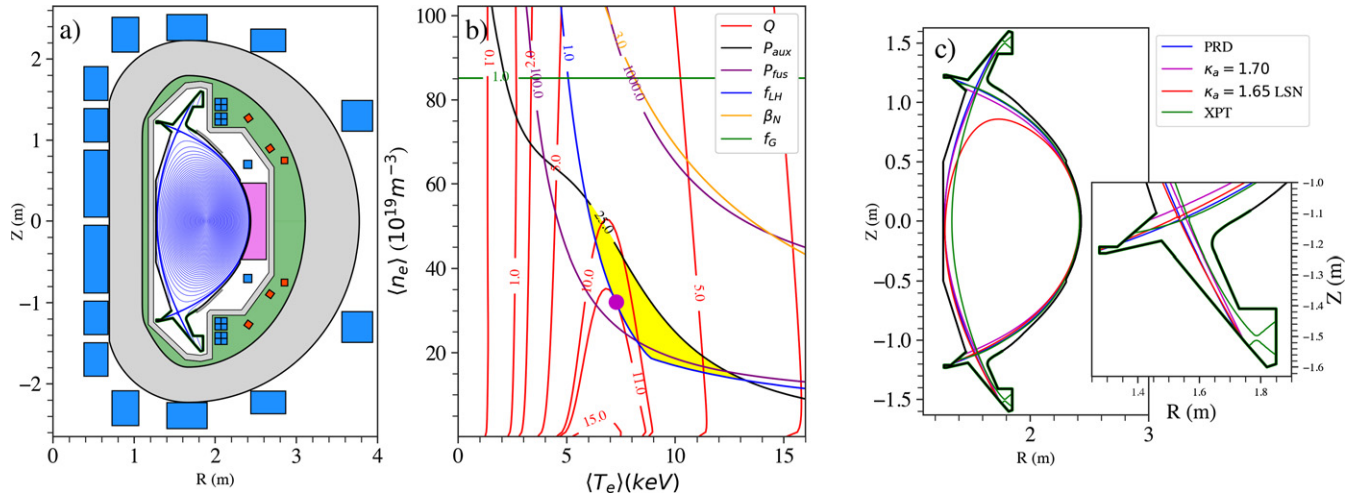
Figure 1. (*a*) SPARC poloidal cross-section. (*b*) POPCON for SPARC with nominal PRD parameters. Yellow shaded area indicates the operational space for H-mode operation ($f_{LH} > 1$) below the available auxiliary heating power ($P_{ICRF} < 25$ MW). The scenario that maximizes fusion gain ($Q \approx 11$, magenta circle) is well below pressure and density limits. Note that this POPCON utilizes the workflow presented in [7] but differs in that the low-density branch of the L–H threshold power is now taken into account. (*c*) Separatrices of possible plasma shapes within capabilities of the poloidal field coils set and divertor geometry.

The PRD requires only 11.1 MW of ICRF input power, as alpha heating keeps the energy flows above the estimated L–H threshold power [25]. This scenario produces 140 MW of fusion power, and all tokamak systems are being designed to sustain this power level during a 10 s current flattop, including the effects of neutron heating and corresponding requirements for shielding and cooling of the superconducting magnets.

While the PRD scenario amply satisfies the SPARC mission and it has been the discharge that has largely driven the design (as it generally represents the most demanding implications for various engineering systems), there is a number of other scenarios of interest for physics studies and that will be used to build expertise towards the $Q > 2$ milestone, investigate specific physics topics or be used as contingency pathways to achieve breakeven. The large margin that the PRD scenario has with respect to the $Q > 2$ mission means that there is significant contingency in case of degraded confinement or pedestal performance. In fact, operation with a degraded H-mode confinement factor of $H_{98,y2} = 0.7$ (two standard deviations below the database fit) still fulfils the $Q > 2$ mission. Similarly, operation at 12.2 T but with L-mode confinement ($H_{89p} = 1.0$ [26]) can also achieve $Q > 2$, owing to the potential of running at lower density ($\langle n_e \rangle \approx 1.4 \times 10^{20}$ m^{-3}) and high input power ($P_{ICRF} = 21.1$ MW), a condition which is unlikely to result in H-mode due to power requirements associated with the low-density branch of the LH power threshold curve. Even in the case that H-mode is accessible in these conditions, it can be avoided by running in 'unfavourable' grad-B drift using upper single null geometries or by controlling $P_{SOL} < P_{LH}$ through core impurity seeding.

Plasmas with lower areal elongation ($k_a = 1.65$) with a single-null equilibrium are also possible and significantly less demanding for the vertical stability control system and poloidal field coils set. Such scenario is also expected to achieve $Q = 6.5$. Likewise, the poloidal field coils set can also allow the exploration of scenarios with slightly larger inner

and outer gaps (3 cm versus 1 cm in PRD), by decreasing minor radius to $a = 55$ cm. Scenarios at reduced magnetic field may also be of use to the SPARC programme. In particular, scenarios with $B_T = 8.0$ T are easily accessible because the ICRF frequency of 120 MHz is resonant near axis in plasmas with H minority. Although such a scenario only achieves $Q = 1.6$ in H-mode with the assumptions used here, shifting the resonance location to slightly off-axis using $B_T = 8.6$ T, is expected to increase performance enough to reach $Q > 2$ under the same assumptions for the kink safety factor (thus at slightly higher plasma current). This will allow the study of possible fast ion turbulence stabilization effects with off-axis heating of minority populations as well as high-Z impurity control. Plasmas with $B_T = 8.0$ T are also anticipated for early operation with deuterium-only plasmas. As will be discussed in the next section, given the high power requirements for H-mode access at $B_T = 12.2$ T in D–D, operation with 8 T will be needed to study H-mode physics, pedestal formation and transients before introducing tritium in the machine. Figure 1(*c*) presents some characteristic separatrix shapes that the poloidal field coil set is able to produce for SPARC.

4. Core plasma physics

The PRD scenario presented in the previous section represents the most stringent plasma discharge for SPARC and therefore much effort has been devoted to the understanding of the physics of the PRD and the resulting machine engineering requirements.

The PRD is a scenario that leverages conventional H-mode operation to achieve performance goals. This choice does not preclude operation in other high-performance operational regimes but extensive experience with conventional H-mode in tokamak operations makes it a conservative choice for projecting SPARC performance. Due to the lack of first-principles models for the low-to high-confinement transition
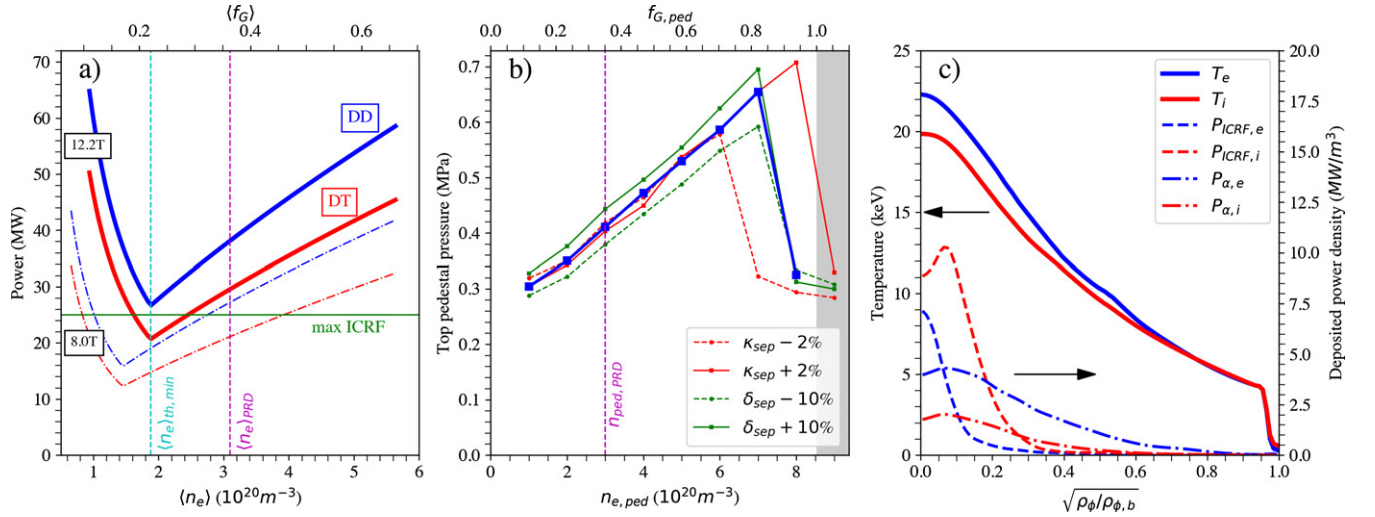
Figure 2. (*a*) L–H threshold power versus density for D–D and D–T full-field (12.2 T) and reduced-field (8.0 T) plasmas, using the ITPA scaling [25] and isotope correction [27]. Increased power at low densities is accounted for with an ad-hoc model following reference [12] of $\left(n_{\min}/n\right)^2$, with $n_{\min}$ calculated as in [28]. (*b*) EPED predictions for the top pedestal pressure versus pedestal density, including scans of shaping parameters (expected during divertor strike point sweep) around nominal operation. (*c*) Electron and ion temperature profiles and deposited power density for each species from ICRF and alpha heating.

(L–H power threshold), an empirical scaling-law [25, 27] approach has been taken to project H-mode access in SPARC [12], as shown in figure 2(*a*). At 12.2 T, the minimum power required to access H-mode in D–T plasmas is projected to be $P_{th} = 21$ MW and occur near $n_e \approx 1.9 \times 10^{20}$ m^{-3} [28]. The total auxiliary power installed in SPARC is in excess of this value ($P_{ICRF} = 25$ MW) and given the non-negligible alpha heating that may occur in L-mode, it is then inferred that SPARC will likely be able to access H-mode in its full-field D–T scenario. Access in less stringent scenarios, such as 8 T, are also possible and will be explored in the pre-nuclear phase of SPARC to characterize H-mode operation and extend the databases to close gaps in our projections to pilot plants. During the H-mode phase, the increased density will raise the power requirements, and thus it is expected that significant alpha heating will be required to sustain robust H-mode operation. SPARC will feature a gas-fueling system as baseline fuelling actuator, but the implementation of pellet injectors will not be precluded.

MHD stability analysis with the EPED model [29] (shown in figure 2(*b*)) indicates that SPARC will operate mostly with pedestals that are peeling limited, owing to the low normalized density and the strong shaping of the PRD scenario. The transition to the ballooning branch occurs at significantly higher density or lower elongation, and therefore a degradation of the pedestal pressure with density, signature of ballooning-limited pedestals, is not expected. Pedestal performance is therefore favourable to upward excursions in density from the PRD nominal operation. Analysis of the sensitivity of the pedestal predictions to changes in plasma parameters such as elongation, triangularity, normalized pressure and pedestal density has been performed in references [11, 12], demonstrating that the solution is robust to expected variations in plasma parameters.

As presented in reference [11], an advanced integrated modelling approach has been utilized to predict plasma kinetic profiles and associated plasma performance. Figure 2(*c*) shows the temperature and deposited power density profiles predicted for the PRD using the TRANSP [30] power balance framework coupled to the TGLF-SAT1 [31] model for turbulent transport. Pedestal pressure as given by EPED has been used as a boundary condition, and pedestal density is chosen so as to achieve an operational volume-average density of $\langle n_e \rangle = 3.1 \times 10^{20}$ m^{-3}. Predicted performance of this scenario is $Q \approx 9$, remarkably close to the empirical predictions with POPCON analysis with the same amount of auxiliary heating power. The TGLF gyro-fluid turbulence model indicates that SPARC will be dominated by ion-scale ion temperature gradient (ITG) modes, with some unstable electron-scale modes in further out regions of the plasma. Even though the PRD scenario is mostly electron heated, radiation is the dominant heat exhaust mechanism for the electron energy channel, leading to heat flux ratios of the order of $Q_i/Q_e \sim 2$–3 throughout the entire plasma core, as is often the case in today's neutral beam ion (NBI) heated discharges. Nonetheless, SPARC will not have external torque input (no NBI) and SPARC discharges will predominantly feature moderate to low toroidal rotation. Empirical predictions of SPARC intrinsic torque and rotation have been performed [32]. An intrinsic torque of $\sim$4 Nm is predicted, leading to a core Mach number of $\mathcal{M} \sim 0.16$.

Extensive gyrokinetic analysis of the SPARC PRD scenario has been carried out in reference [33]. Gyro-fluid modelling results are confirmed with linear and nonlinear CGYRO [34] simulations of the core of SPARC. Long-wavelength ITG has a dominant role throughout the core, although presence of sub-dominant trapped electron mode turbulence is found in outer radii. The contribution of short wavelength turbulence to the total heat fluxes is estimated to be minimal, and electromagnetic fluctuations and the inclusion of toroidal rotation (at levels empirically estimated [32]) are found to have a favourable effect through stabilization of the

ITG turbulence. High-Z core impurity accumulation has been assessed through scans of the impurity gradient scale length in nonlinear gyrokinetic and neoclassical transport simulations, revealing peaking factors that do not imply dangerous accumulation up to $\rho = 0.4$ [33]. Future work will extend such analysis to the near-axis region and will include other operational scenarios. The possibly favourable effect of fast ions from off-axis ICRF minorities [35] is currently being evaluated, which could lead to the attainment of the $Q > 2$ mission and burning plasmas at lower magnetic field and plasma current by means of improving energy confinement.

SPARC net energy gain mission will be achieved with ICRF as the sole auxiliary heating mechanism. In particular, minority heating scenarios with fast wave at 120 MHz will be used for optimal absorption and bulk ion heating at both full (12.2 T) and reduced (8.0 T) on-axis magnetic fields. An antenna spectrum of $k_\parallel \sim 15$–18 m^{-1} has been found to provide a balance of good edge coupling and core absorption, as described in detail in reference [14]. Methods to prevent contamination of the plasma with high-Z impurities at high ICRF power operation have been taken into account during the design of SPARC antennae. These include the use of four-strap, field-aligned antennae with low power density, following extensive experimental experience in Alcator C-Mod and ASDEX Upgrade. Even though the PRD scenario requires 11.1 MW of ICRF power during the high-gain H-mode flattop, a total of 25 MW of coupled power will be available (driven by H-mode access requirements in D–D). A D–T(^{3}He) scheme is used for nominal operation in PRD with 5% ^{3}He concentration. In this regime, 80% of the ICRF power is damped by the fast ^{3}He (fundamental resonance), as predicted by TORIC [36] and FPPMOD [37]. After slowing down, bulk ion species receive 78% of the total ICRF coupled power. The commissioning and demonstration of SPARC ICRF system will occur with scenarios at 8.0 T and 12.2 T, utilizing H-minority heating and ^{3}He-minority heating in ^{4}He main-ion plasmas.

Access to high fusion power and burning plasmas regimes in SPARC will produce significant amounts of energetic alpha particles. This fast alpha population, along with the hot ICRF minority ion tail, poses a potential risk of damage to the first wall and other tokamak systems if significant losses occur due to classical orbit effects and MHD instabilities [16]. Research has focussed on ripple-induced losses, as they can drive the engineering design of the toroidal field magnets and may influence the design of the limiter surfaces and plasma facing components (PFCs). Work with ASCOT [38] and SPIRAL [39] has shown that magnetic field ripple from perfectly aligned coils (0.15% nominal edge ripple) does not cause a significant peak surface power density (<250 kW m^{-2}), and are sub-dominant to neoclassical first-orbit losses (2.8%), as described in [16]. Simulations with imperfectly manufactured and imperfectly positioned coils are being used during the design of an optimized wall shape, as well as the ICRF antennas and limiter locations [16]. Because of their low toroidal mode number magnetic field perturbation, we expect the alpha losses associated with the effect of the error field correction coils (EFCCs) to be small compared to ripple-induced losses. Even though the latter are already expected to be small, future work will explore the combined effect of the toroidal field coils misalignments and EFCC on fast ion populations in SPARC.

5. Plasma facing components and heat flux handling

The compact size, high magnetic field and high power density in SPARC will produce reactor-class divertor conditions, and therefore will serve as a testbed to benchmark empirical scalings, computational models and mitigation strategies suited for fusion power plants. Empirical scalings of the heat flux width [40] yield $\lambda_q \approx 0.3$ mm (regression #15) mapped to the outer midplane, resulting in a peak unmitigated parallel heat flux of $q_\parallel > 6$ GW m^{-2} at the SPARC divertor target plates [41] for the PRD scenario ($P_{sol} = 29$ MW). The surface heat flux profiles have been estimated for the inner and outer divertor targets assuming toroidally symmetric target plates, resulting in $\sim$100 MW m^{-2} of peak heat flux for both inner and outer divertors, with an incidence angle of $\alpha \approx 0.95°$. Tile shaping to eliminate leading edges is estimated to increase the peak values by 50%. On account of the desired simplicity for the design and construction of SPARC and the limited overall lifetime, the divertor is being designed to withstand these heat loads without active cooling, without remote handling and using established PFC materials. A key challenge is overcoming the lack of maintenance in a radiation environment once nuclear operations have begun, as both sustained D–D and D–T operations pose a health safety risk. Unlike many existing devices, but similar to ITER, SPARC is not planning a multi-campaign deployment or upgrade strategy for its PFCs.

The decision to use tungsten-based materials for the PFCs has recently been made, after a careful consideration of tradeoffs between low- and high-Z material options and associated risks, since many areas of plasma physics and tokamak systems are impacted. Carbon-based PFC materials would be preferred for meeting SPARC's mission goals due to improved manufacturability, reduced eddy current torques and increased resistance to damage from thermal transients, relative to tungsten. However, the tritium retention and high erosion rates in carbon-based materials do not project well towards a pilot plant, and would create a risk for the timely achievement of SPARC's goals within limited tritium inventory. Therefore, SPARC will feature a divertor made of tungsten-based tiles.

Attributable to the gap between current experiments and SPARC divertor conditions, it is not possible to ensure that SPARC will be able to achieve a detached divertor that is compatible with high core confinement. Therefore, SPARC is being designed under the conservative assumption of moderately dissipative divertor conditions, assuming $\sim$50% of the power leaving the LCFS is removed volumetrically before reaching the divertor. Power-sharing fractions assumed will be consistent with single-null equilibrium for divertor considerations, with a 60/40 outer/inner split, even though SPARC is being designed to produce up-down symmetric equilibria. The PRD scenario will leverage the flexibility of the poloidal field and divertor coils to produce a $\sim$1 Hz strike point sweep during the 10 s flattop to spread the heat flux over a large surface area in order to keep divertor tile surface temperatures within
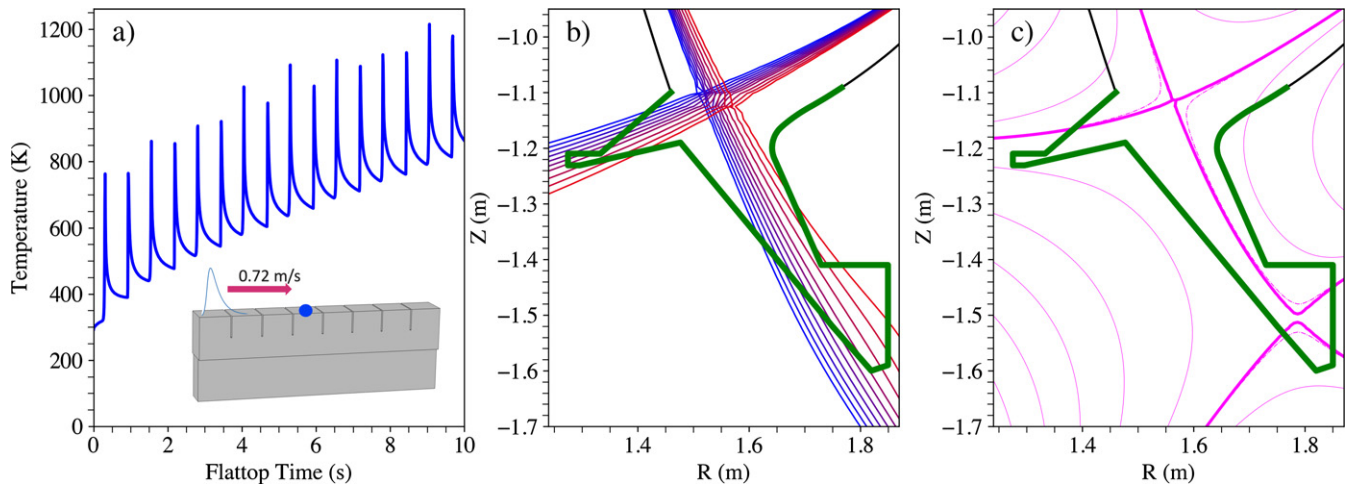
Figure 3. (*a*) PFC surface temperature as a function of time over a 10 s flattop using a simplified COMSOL thermal model of the outer divertor strike point sweep. (*b*) Equilibria evolution during strike point sweep (only separatrices are shown) and (*c*) XPT equilibrium, both obtained using FreeGS [48] with SPARC current poloidal field coil set capabilities.

limits without active cooling systems, as shown in figures 3(*a*) and (*b*). By doing so, the surface temperature of the PFC spikes locally with each pass of the strike point, but conduction into the bulk material ensures that melt temperatures for tungsten will not be reached. While avoiding melt is possible, short term surface temperature excursions above the recrystallization limit will be encountered in SPARC and are unavoidable during sweeping control failures, high powered edge localized modes (ELMs) and disruptions. A key challenge during SPARC operations will be to budget for and monitor damage of the tungsten surface over the device's lifetime. The sweep trajectories are being optimized to match the capabilities of the power supply systems. Modelling work with UEDGE [42] and SOLPS-ITER [43] is underway to predict divertor and edge conditions and identify impurity seeding and detachment requirements for the high-power scenarios [44, 45].

SPARC will be used to explore potential solutions for achieving and controlling detached divertors at conditions relevant for fusion pilot plants. A dedicated advanced divertor mission, which complements the primary $Q > 2$ mission, drives device design and diagnostic requirements. The coil systems and divertor shapes are being designed to study double-null, long-legged and X-point target (XPT) divertor configurations, which have been proposed in the design of compact pilot plants [9] due to the wide detachment power window. Although the XPT scenario will not be able to run at full plasma current ($I_p \leqslant 5.7$ MA), it is still expected $Q > 2$ and substantial fusion power ($P_{fus} = 37$ MW) [7], resulting in a unique platform to study advanced divertor scenarios. Figure 3(*c*) depicts one possible XPT scenario. In particular, SPARC will explore the effect of the secondary null location on power dissipation, as well as the sensitivity of the detachment location and dissipation to the external controls and transients. Modelling of the XPT configuration with UEDGE is underway, as well as the evaluation of the requirements for X-point position control [46]. Many of the topics addressed by the advanced divertor mission parallel those identified by the fusion community [47], although there is an emphasis on

obtaining the minimum viable information necessary to inform ARC, which necessarily limits the measurement capabilities.

Unmitigated Type-I ELM frequencies of 3–15 Hz have been projected, with a peak parallel energy fluence of 11–32 MJ m^{-2} to the divertor [12, 13], similar to ITER projections [49], although surface heat flux loads are presently envisioned to be smaller due to a lower angle of incidence. Estimated divertor ELM thermal loads result in heat flux factors between 3.7–39 MJ m^{-2} s$^{-1/2}$ over large fractions of the divertor surface which will allow for exposure from one to a few ELMs. To expand the H-mode operation window, increase margin and ensure survivability of the divertor PFCs, extrinsic ELM mitigation tools are being considered by the SPARC team. The feasibility and requirements for pellet injection [50], resonant magnetic perturbations [51] and plasma jogs [52] are currently being evaluated. At the same time, small-ELM and intrinsically ELM-suppressed regimes [53] (such as I-mode [54] and QH-mode [55]) are also being considered. Although both extrinsic and intrinsic mitigation techniques often lead to reduced pedestal pressure, given the large margin that the PRD scenario has to the $Q > 2$ mission, it is expected that SPARC will readily meet its primary mission even with the reduced confinement associated with lower pedestal performance.

The transient loading to the divertor surface from the unmitigated thermal quench of disruptions in PRD scenarios has been estimated to produce heat flux factors of up to 1–2 GJ m^{-2} s$^{-1/2}$ [41], when uncertainties in physics parameters are propagated. Such an event will push any material limits and will cause top-surface melting of tungsten. Disruption mitigation will be utilized, but the high power density may still result in main-chamber PFCs seeing heat flux factors of several tens of MJ m^{-2} s$^{-1/2}$, depending on toroidal and poloidal peaking of the thermal quench. The effect of these high transient thermal loads in the bulk PFC is being assessed through computational modelling and testing of plasma facing material. Nonetheless, the SPARC team is focussing on disruption mitigation techniques to avoid these problematic situations, as will be described in the next section.
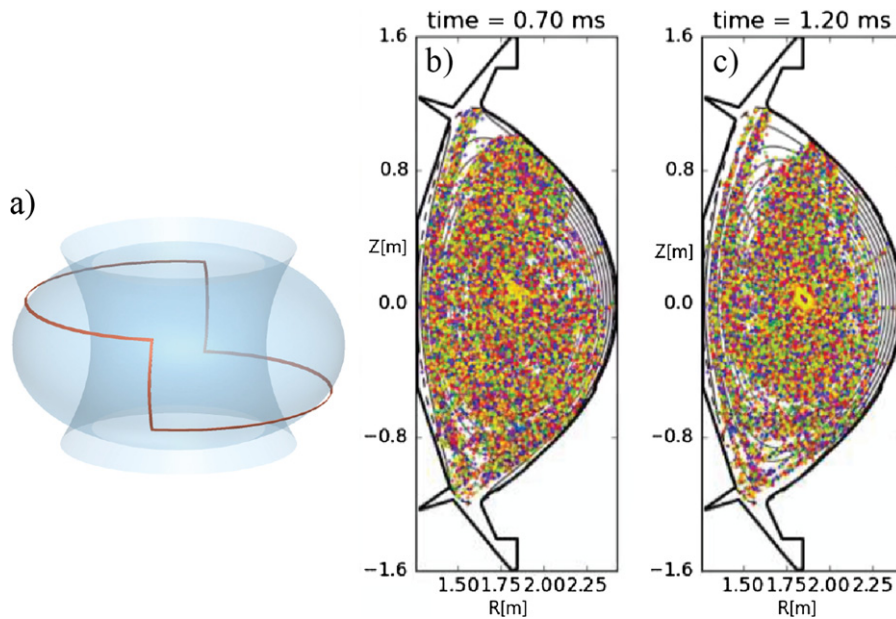
Figure 4. (*a*) Outboard-side passive REMC with dominantly $n = 1$ character under design for SPARC. (*b*) Poincare plot showing the stochastic field distribution 0.70 ms and (*c*) 1.2 ms after the thermal quench. Note the $80\%-20\%$ current quench duration in this simulation is 3.2 ms.

6. Stability and disruptions

The use of high magnetic fields opens a wide window of high-performance operation with comfortable margins to disruption limits. In particular, the low normalized beta ($\beta_N \approx 1.05$), low normalized density ($f_G \approx 0.37$) and moderate safety factor ($q_{95} \approx 3.4$) of the PRD scenario reduce instability drives, resulting in an expected lower frequency of disruptions [15]. Nonetheless, the disruption loading in SPARC is comparable to ITER and therefore all tokamak systems are being designed with a level of passive resilience suitable to withstand the predicted loads from a realistic number of both mitigated and unmitigated disruptions.

The compact size of SPARC results in short thermal quench and current quench durations, with empirically estimated lower bounds of $\geqslant 50~\mu s$ [56] and $\geqslant 3.2$ ms [57] respectively. Although empirical scalings suggest a possible favourable effect of the toroidal field (as they often have Alcator C-Mod, with a field of up to 8 T, as an outlier), the engineering design of SPARC will not take credit for this and instead will utilize empirical probability distributions for the quench durations.

Similarly, SPARC structures are being designed to withstand the highest predicted forces and torques caused by eddy currents. SPARC plasma-facing component design is working to trade-off reducing eddy current torques in plasma facing material by reducing unit size and increasing unique part count by making tiles overly small. Larger first-wall components such as limiter and divertor support structures, ICRF antennas, ports and vacuum vessel are being engineered to withstand these loads. Peak halo currents of substantial

fractions of the plasma current (up to 50% with peaking factors of 1.4 in rare events) are expected following vertical displacements events [57]. High unattenuated, axisymmetric vertical forces of up to 35 MN [58] could be possible. The vacuum vessel is also being engineered accounting for these loads, with multi-physics analysis to examine in detail the electromechanical loads (in particular, contact points and halo current paths).

Runaway electrons (REs) pose an important challenge for tokamak operations and ARC survival, and SPARC has multiple advantages as a facility to study solutions to this problem at reactor scale. Even though modelling work suggest a favourable effect of the high elongation in SPARC [59], they can cause serious damage to PFC materials. However, SPARC does not have actively cooled PFCs, and can endure damage from REs without risking loss of coolant accidents. The design of a passive runaway electron mitigation coil (REMC) is underway, as modelling results are very encouraging. The REMC is able to mitigate or even suppress the runaway seed by applying three-dimensional non-axisymmetric error fields that deconfine REs by breaking up flux surfaces into widespread stochasticity [60]. Time-dependent magnetic fields from COMSOL simulations of various REMC configurations are provided for nonlinear MHD modelling with NIMROD [61]. Recent simulations show that a coil with dominant $n = 1$ toroidal mode number perturbations (as the one shown in figure 4(*a*)) drives a stochastic loss rate that exceeds the avalanche growth rate, preventing exponentiation of very small seed populations. Figures 4(*b*) and (*c*) show the long-lasting stochastic field distribution after the thermal quench. Work is on-going to assess the full evolution of the RE beam

and the integration of the REMC in the tokamak, including its compatibility with plasma initiation.

SPARC will begin operations using massive gas injection for disruption mitigation, but is being designed to enable testing of other mitigation techniques as future upgrades. Regardless of the approach, to trigger the mitigation actuators in a timely manner, work is underway to develop disruption prediction algorithms that can provide warnings in real time prior to the thermal quench. The SPARC team is leveraging datadriven algorithms [62, 63] to robustly predict transitions to unstable operational spaces, following the success of similar techniques in current devices, achieving >90% of true positive rates in some machines [64]. Transfer learning techniques to leverage existing data to extrapolate to SPARC are being evaluated [65].

7. Conclusions

SPARC aims to be a demonstration device for the highfield path to economical fusion energy. It is on track to start construction in the second half of 2021 following the demonstration of a TFMC manufactured from high-temperature superconductor tapes. This paper has described progress in the plasma physics basis and engineering design of the SPARC tokamak as it stands at the time of submission.

The regimes and scenarios that SPARC is projected to access represent a major opportunity to benchmark and further extend the validation of plasma physics models to reactorrelevant regimes of tokamak operations, closing the gap in the projections and reducing risk for fusion pilot plant designs. While the design of SPARC is largely based on conservative assumptions, the design of ARC-class devices requires the relaxation of some of these assumptions [13] and therefore burning plasma experiments like SPARC and ITER are of critical importance for reducing the uncertainties associated with the design of a fusion pilot plant and to gain experience with reactor-relevant tokamak operations. The high-field path facilitates fast-paced iterations at reduced cost (due to the compact size) that are key to find the optimal pathway to bring economical fusion energy to the world in a timely manner.

Acknowledgments

ORCID iDs

P. Rodriguez-Fernandez https://orcid.org/0000-0002-7361-1131
A.J. Creely https://orcid.org/0000-0002-4464-150X
M.J. Greenwald https://orcid.org/0000-0002-4438-729X
S.B. Ballinger https://orcid.org/0000-0003-3593-6418
C.P. Chrobak https://orcid.org/0000-0002-8177-4416
D.T. Garnier https://orcid.org/0000-0002-0718-1073
R. Granetz https://orcid.org/0000-0002-6560-1881
N.T. Howard https://orcid.org/0000-0002-8787-6309
J.W. Hughes https://orcid.org/0000-0003-4802-4944
V.A. Izzo https://orcid.org/0000-0002-4198-4726
A.Q. Kuang https://orcid.org/0000-0002-8917-2911
C. Rea https://orcid.org/0000-0002-9948-2649
M.L. Reinke https://orcid.org/0000-0003-4413-9613
V. Riccardo https://orcid.org/0000-0003-2535-5257
J.E. Rice https://orcid.org/0000-0001-8319-5971
S.D. Scott https://orcid.org/0000-0002-3132-3692
B.N. Sorbom https://orcid.org/0000-0002-2110-6766
J.A. Stillerman https://orcid.org/0000-0003-0901-0806
R. Sweeney https://orcid.org/0000-0003-3408-1497
R.A. Tinguely https://orcid.org/0000-0002-3711-1834

References

[1] Cohn D.R., Schwartz J., Bromberg L. and Williams J.E.C. 1988 Tokamak reactor concepts using high temperature, high-field superconductors *J. Fusion Energy* **7** 91–4

[2] Whyte D.G., Minervini J., Labombard B., Marmar E., Bromberg L. and Greenwald M. 2016 Smaller & sooner: exploiting high magnetic fields from new superconductors for a more attractive fusion energy development path *J. Fusion Energy* **35** 41–53

[3] National Academies of Sciences, Engineering and Medicine 2019 *Final Report of the Committee on a Strategic Plan for US Burning Plasma Research* (The National Academies Press)

[4] National Academies of Sciences, Engineering and Medicine 2021 *Report of the Committee on the Key Goals and Innovation Needed for a US Fusion Pilot Plant* (The National Academies Press)

[5] American Physical Society Division of Plasma Physics Community Planning Process 2020 A community plan for fusion energy and discovery plasma sciences *Technical Report* (American Physical Society)

[6] Fusion Energy Sciences Advisory Committee 2020 A longrange plan to deliver fusion energy and to advance plasma science

[7] Creely A.J. *et al* 2020 Overview of the SPARC tokamak *J. Plasma Phys.* **86** 865860502

[8] Sorbom B.N. *et al* 2015 ARC: a compact, high-field, fusion nuclear science facility and demonstration power plant with demountable magnets *Fusion Eng. Des.* **100** 378–405

[9] Kuang A.Q. *et al* 2018 Conceptual design study for heat exhaust management in the ARC fusion pilot plant *Fusion Eng. Des.* **137** 221–42

[10] Mumgaard R. (SPARC Team) 2018 SPARC and the high-field path to commercial fusion energy *60th Annual Meeting of the*

APS Division of Plasma Physics (Portland, OR, 5-9 November 2018) (https://www-internal.psfc.mit.edu/research/alcator/pubs/APS/APS2018/Mumgaard_APS_20108.pdf)

[11] Rodriguez-Fernandez P., Howard N. T., Greenwald M. J., Creely A. J., Hughes J. W., Wright J. C., Holland C., Lin Y. and Sciortino F. (The SPARC Team) 2020 Predictions of core plasma performance for the SPARC tokamak *J. Plasma Phys.* **86** 865860503

[12] Hughes J.W., Howard N.T., Rodriguez-Fernandez P., Creely A.J., Kuang A.Q., Snyder P.B., Wilks T.M., Sweeney R. and Greenwald M. 2020 Projections of H-mode access and edge pedestal in the SPARC tokamak *J. Plasma Phys.* **86** 865860504

[13] Kuang A.Q. *et al* 2020 Divertor heat flux challenge and mitigation in SPARC *J. Plasma Phys.* **86** 865860505

[14] Lin Y., Wright J.C. and Wukitch S.J. 2020 Physics basis for the ICRF system of the SPARC tokamak *J. Plasma Phys.* **86** 865860506

[15] Sweeney R. *et al* 2020 MHD stability and disruptions in the SPARC tokamak *J. Plasma Phys.* **86** 865860507

[16] Scott S.D., Kramer G.J., Tolman E.A., Snicker A., Varje J., Särkimäki K., Wright J.C. and Rodriguez-Fernandez P. 2020 Fast-ion physics in SPARC *J. Plasma Phys.* **86** 865860508

[17] Hartwig Z.S. *et al* 2020 VIPER: an industrially scalable high-current high-temperature superconductor cable *Supercond. Sci. Technol.* **33** 11LT01

[18] Salazar E.E. *et al* 2021 Fiber optic quench detection for large-scale HTS magnets demonstrated on VIPER cable during high-fidelity testing at the SULTAN facility *Supercond. Sci. Technol.* **34** 035027

[19] Molodyk A. *et al* 2021 Development and large volume production of extremely high current density $YBa_2Cu_3O_7$ superconducting wires for fusion *Sci. Rep.* **11** 2084

[20] French J.W., Fedor B.J., Shaw L.E. and Sabado M.M. 1983 Construction of the tokamak fusion test reactor *Nucl. Technol./Fusion* **4** 326–35

[21] Keilhacker M., Gibson A., Gormezano C. and Rebut P.H. 2001 The scientific success of JET *Nucl. Fusion* **41** 1925–66

[22] Commonwealth Fusion Systems 2021 Commonwealth fusion systems selects 47-acre site in Devens, mass., for historic commercial fusion energy campus (https://cfs.energy/news-and-media/commonwealth-fusion-systems-selects-47-acre-site-in) (cfs.energy)

[23] Houlberg W.A., Attenberger S.E. and Hively L.M. 1982 Contour analysis of fusion reactor plasma performance *Nucl. Fusion* **22** 935–45

[24] ITER Physics Basis Expert Groups on Confinement and Transport and Confinement Modelling and Database, ITER Physics Basis Editors 1999 Chapter 2: plasma confinement and transport *Nucl. Fusion* **39** 2175

[25] Martin Y.R. and Takizuka T. (ITPA CDBM H-Mode Threshold Database Working Group) 2008 Power requirement for accessing the H-mode in ITER *J. Phys.: Conf. Ser.* **123** 012033

[26] Yushmanov P.N., Takizuka T., Riedel K.S., Kardaun O J.W.F., Cordey J.G., Kaye S.M. and Post D.E. 1990 Scalings for tokamak energy confinement *Nucl. Fusion* **30** 1999–2006

[27] Behn R., Labit B., Duval B.P., Karpushov A., Martin Y. and Porte L. 2014 Threshold power for the transition into H-mode for H, D, and He plasmas in TCV *Plasma Phys. Control. Fusion* **57** 025007

[28] Ryter F., Barrera Orte L., Kurzan B., Mcdermott R.M., Tardini G., Viezzer E., Bernert M. and Fischer R. (The ASDEX Upgrade Team) 2014 Experimental evidence for the key role of the ion heat channel in the physics of the L−H transition *Nucl. Fusion* **54** 083003

[29] Snyder P.B., Groebner R.J., Hughes J.W., Osborne T.H., Beurskens M., Leonard A.W., Wilson H.R. and Xu X.Q. 2011 A first-principles predictive model of the pedestal height and width: development, testing and ITER optimization with the EPED model *Nucl. Fusion* **51** 103016

[30] Breslau J., Gorelenkova M., Poli F., Sachdev J. and Yuan X. 2018 *TRANSP. Computer Software* (USDOE Office of Science) (https://www.osti.gov/biblio/1489900-transp)

[31] Staebler G.M., Howard N.T., Candy J. and Holland C. 2017 A model of the saturation of coupled electron and ion scale gyrokinetic turbulence *Nucl. Fusion* **57** 066046

[32] Rice J.E. *et al* 2021 Dimensionless parameter scaling of intrinsic torque in C-Mod enhanced confinement plasmas *Nucl. Fusion* **61** 026013

[33] Howard N.T., Rodriguez-Fernandez P., Holland C., Rice J.E., Greenwald M.J., Candy J. and Sciortino F. 2021 Gyrokinetic simulation of turbulence and transport in the SPARC tokamak *Physics of Plasmas* **28** 072502

[34] Candy J., Belli E.A. and Bravenec R.V. 2016 A high-accuracy Eulerian gyrokinetic solver for collisional plasmas *J. Comput. Phys.* **324** 73–93

[35] Di Siena A., Görler T., Poli E., Navarro A.B., Biancalani A. and Jenko F. 2019 Electromagnetic turbulence suppression by energetic particle driven modes *Nucl. Fusion* **59** 124001

[36] Brambilla M. 1999 Numerical simulation of ion cyclotron waves in tokamak plasmas *Plasma Phys. Control. Fusion* **41** 1–34

[37] Hammett G.W. 1986 Fast ion studies of ion cyclotron heating in the PLT tokamak *PhD Thesis* Princeton University

[38] Varje J., Särkimäki K., Kontula J., Ollus P., Kurki-Suonio T., Snicker A., Hirvijoki E. and Äkaslompolo S. 2019 High-performance orbit-following code ASCOT5 for Monte Carlo simulations in fusion plasmas (arXiv:1908.02482v1)

[39] Kramer G.J., Budny R.V., Bortolon A., Fredrickson E.D., Fu G.Y., Heidbrink W.W., Nazikian R., Valeo E. and Van Zeeland M.A. 2013 A description of the full-particle-orbit-following SPIRAL code for simulating fast-ion experiments in tokamaks *Plasma Phys. Control. Fusion* **55** 025013

[40] Eich T. *et al* 2013 Scaling of the tokamak near the scrape-off layer H-mode power width and implications for ITER *Nucl. Fusion* **53** 093031

[41] Kuang A.Q. *et al* (SPARC TEAM) 2021 The divertor challenge anticipated for SPARC *24th Int. Conf. on Plasma Surface Interaction in Fusion Devices* (Virtual Meeting, 24-29 January 2021) (https://mmm2020.kr/)

[42] Rognlien T.D., Milovich J.L., Rensink M.E. and Porter G.D. 1992 A fully implicit, time dependent 2-D fluid code for modeling tokamak edge plasmas *J. Nucl. Mater.* **196–198** 347–51

[43] Wiesen S. *et al* 2015 The new SOLPS-ITER code package *J. Nucl. Mater.* **463** 480–4

[44] Ballinger S.B., Kuang A.Q., Umansky M.V., Brunner D., Canik J.M., Greenwald M.J., Lore J.D., LaBombard B., Terry J.L. and Wigram M. the SPARC Team 2021 Simulation of the SPARC plasma boundary with the UEDGE code *Nucl. Fusion* **61** 086014

[45] Lore J., Canik J.M., Kuang A.Q., Labombard B., Lipschultz B. and Reinke M.L. 2020 Predictive modeling of SPARC divertor conditions using SOLPS-ITER *62nd Annual Meeting of the APS DPP, Abstract BP13.00004* (Virtual Conference, 9-13 November 2020) (https://meetings.aps.org/Meeting/DPP20/Session/BP13.4https://meetings.aps.org/Meeting/DPP20/Session/BP13.4)

[46] Kolemen E., Gates D.A., Gerhardt S., Kaita R., Kugel H., Mueller D., Rowley C. and Soukhanovskii V. 2011 Plasma modelling results and shape control improvements for NSTX *Nucl. Fusion* **51** 113024

[47] Maingi R., Zinkle S.J. and Foster M.S. 2015 *Fusion Energy Sciences Workshop on Plasma Materials Interactions: Report on Science Challenges and Research Opportunities in Plasma Materials Interactions* (United States: Nuclear Physics)

[48] Dudson B. 2017 FreeGS: free boundary Grad–Shafranov solver (https://github.com/bendudson/freegs)

[49] Eich T., Sieglin B., Thornton A.J., Faitsch M., Kirk A., Herrmann A. and Suttrop W. 2017 ELM divertor peak energy fluence scaling to ITER with data from JET, MAST and ASDEX upgrade *Nucl. Mater. Energy* **12** 84–90

[50] Lang P.T. *et al* 2004 ELM pace making and mitigation by pellet injection in ASDEX upgrade *Nucl. Fusion* **44** 665–77

[51] Evans T.E. *et al* 2004 Suppression of large edge-localized modes in high-confinement DIII-D plasmas with a stochastic magnetic boundary *Phys. Rev. Lett.* **92** 235003

[52] De La Luna E. *et al* (JET Contributors) 2016 Understanding the physics of ELM pacing via vertical kicks in JET in view of ITER *Nucl. Fusion* **56** 026001

[53] Viezzer E. 2018 Access and sustainment of naturally ELM-free and small-ELM regimes *Nucl. Fusion* **58** 115002

[54] Whyte D.G. *et al* (The Alcator C-MOD Team) 2010 I-mode: an H-mode energy confinement regime with L-mode particle transport in Alcator C-Mod *Nucl. Fusion* **50** 105005

[55] Burrell K.H. *et al* 2004 Edge radial electric field structure in quiescent H-mode plasmas in the DIII-D tokamak *Plasma Phys. Control. Fusion* **46** A165

[56] ITER Physics Expert Group on Disruptions, Plasma Control, and MHD and ITER Physics Basis Editors 1999 Chapter 3: MHD stability, operational limits and disruptions *Nucl. Fusion* **39** 2251–389

[57] Eidietis N.W. *et al* 2015 The ITPA disruption database *Nucl. Fusion* **55** 063030

[58] Miyamoto S. 2011 A linear response model of the vertical electromagnetic force on a vessel applicable to ITER and future tokamaks *Plasma Phys. Control. Fusion* **53** 082001

[59] Fülöp T., Helander P., Vallhagen O., Embreus O., Hesslow L., Svensson P., Creely A.J., Howard N.T. and Rodriguez-Fernandez P. 2020 Effect of plasma elongation on current dynamics during tokamak disruptions *J. Plasma Phys.* **86** 474860101

[60] Boozer A.H. 2011 Two beneficial non-axisymmetric perturbations to tokamaks *Plasma Phys. Control. Fusion* **53** 084002

[61] Sovinec C.R. *et al* (The NIMROD Team) 2004 Nonlinear magnetohydrodynamics simulation using high-order finite elements *J. Comput. Phys.* **195** 355

[62] Rea C., Montes K.J., Erickson K.G., Granetz R.S. and Tinguely R.A. 2019 A real-time machine learning-based disruption predictor in DIII-D *Nucl. Fusion* **59** 096016

[63] Montes K.J. *et al* 2019 Machine learning for disruption warnings on Alcator C-Mod, DIII-D, and EAST *Nucl. Fusion* **59** 096015

[64] Kates-Harbeck J., Svyatkovskiy A. and Tang W. 2019 Predicting disruptive instabilities in controlled fusion plasmas through deep learning *Nature* **568** 526–31

[65] Zhu J.X., Rea C., Montes K., Granetz R.S., Sweeney R. and Tinguely R.A. 2021 Hybrid deep-learning architecture for general disruption prediction across multiple tokamaks *Nucl. Fusion* **61** 026007